

Toward Generalizable Forgery Detection and Reasoning

Yueying Gao, Dongliang Chang, Bingyao Yu, Haotian Qin, Muxi Diao,
Lei Chen, *Member, IEEE*, Kongming Liang, and Zhanyu Ma, *Senior Member, IEEE*

Abstract—Accurate and interpretable detection of AI-generated images is essential for mitigating risks associated with AI misuse. However, the substantial domain gap among generative models makes it challenging to develop a generalizable forgery detection model. Moreover, since every pixel in an AI-generated image is synthesized, traditional saliency-based forgery explanation methods are not well suited for this task. To address these challenges, we formulate detection and explanation as a unified Forgery Detection and Reasoning task (FDR-Task), leveraging Multi-Modal Large Language Models (MLLMs) to provide accurate detection through reliable reasoning over forgery attributes. To facilitate this task, we introduce the Multi-Modal Forgery Reasoning dataset (MMFR-Dataset), a large-scale dataset containing 120K images across 10 generative models, with 378K reasoning annotations on forgery attributes, enabling comprehensive evaluation of the FDR-Task. Furthermore, we propose FakeReasoning, a forgery detection and reasoning framework with three key components: 1) a dual-branch visual encoder that integrates CLIP and DINO to capture both high-level semantics and low-level artifacts; 2) a Forgery-Aware Feature Fusion Module that leverages DINO’s attention maps and cross-attention mechanisms to guide MLLMs toward forgery-related clues; 3) a Classification Probability Mapper that couples language modeling and forgery detection, enhancing overall performance. Experiments across multiple generative models demonstrate that FakeReasoning not only achieves robust generalization but also outperforms state-of-the-art methods on both detection and reasoning tasks.

Index Terms—Forgery Detection, Multi-Modal Large Language Model, Visual Reasoning, Attention Mechanism.

I. INTRODUCTION

THE rapid advancement of deep generative models has enabled AI to produce highly realistic images, raising concerns about AI misuse, particularly in political propaganda [1], financial fraud [2], and social media manipulation [3]. Accurate and interpretable detection of AI-generated images is essential for mitigating these risks. However, traditional detection methods face two key challenges. First, AI-generated images from different models exhibit distinctive artifacts, leading to a substantial domain gap that limits the generalization ability of detectors relying on generator-specific low-level features. Second, unlike image manipulation methods that modify only specific regions, every pixel in an AI-generated image is synthesized, rendering saliency-based explainability

methods [4]–[7] ineffective. These challenges highlight the need for a generalizable and interpretable AI-generated image detector capable of understanding forgery attributes beyond model-specific patterns.

Prior research has attempted to address these issues using two primary strategies: 1) low-level feature analysis focuses on detecting common fingerprints present across generative models [8]–[11], but these methods suffer from severe domain shift, as training on one set of generative models does not generalize well to unseen model sets; 2) high-level semantics has recently been explored using Vision-Language Models (VLMs) to detect semantics inconsistencies within AI-generated images [12]–[14]. However, due to image-text alignment pretraining, they lack sensitivity of fine-grained artifacts, leading to suboptimal detection performance. Furthermore, while MLLMs have demonstrated some ability to explain manipulated images, existing MLLM-based methods [15]–[18] fail to explore their integration with forgery detection task, limiting their potential in forensics analysis.

To overcome these limitations, we propose modeling AI-generated image detection and explanation as a Forgery Detection and Reasoning task (FDR-Task). As shown in Figure 1, the task leverages MLLMs to perform accurate detection through reliable reasoning over forgery attributes. To facilitate this task, we first propose the Multi-Modal Forgery Reasoning Dataset (MMFR-Dataset), a large-scale dataset containing 120K images across 10 generative models, with 378K reasoning annotations on forgery attributes. Leveraging GPT-4o and a customized construction pipeline, we generate comprehensive reasoning annotations via forgery-oriented prompts. Each annotation is organized into structured stages and hierarchical steps to form a coherent chain-of-thought. To the end, MMFR-Dataset provides a foundation for large-scale training and evaluation for MLLM-based forgery detectors.

Building upon the MMFR-Dataset, we propose FakeReasoning, a forgery detection and reasoning framework that enhances both detection accuracy and interpretability. FakeReasoning introduces three key components. First, a dual-branch visual encoder that combines CLIP and DINO is employed to extract both high-level semantics and low-level artifacts, enhancing the fine-grained forgery perception of MLLMs. Second, the Forgery-Aware Feature Fusion module (FAFF) uses DINO’s attention maps as forgery-aware priors and fuses the two-branch visual features through a cross-attention mechanism. This design adaptively guides MLLMs’ attention on low-level and high-level clues while highlighting potential forgery regions and entities. Third, the Classification Probability Mapper (CPM) couples forgery detection with

Y. Gao, D. Chang, H. Qin, M. Diao, K. Lang, and Z. Ma are with the Pattern Recognition and Intelligent System Laboratory, School of Artificial Intelligence, Beijing University of Posts and Telecommunications, Beijing 100876, China. E-mail: {gaoyueying, changdongliang, qinhaotian, dmx, liangkongming, mazhanyu}@bupt.edu.cn

B. Yu and L. Chen are with the Department of Automation, Tsinghua University, Beijing 100084, China. E-mail: {yuby, leichenthu}@tsinghua.edu.cn
Corresponding author: Dongliang Chang.

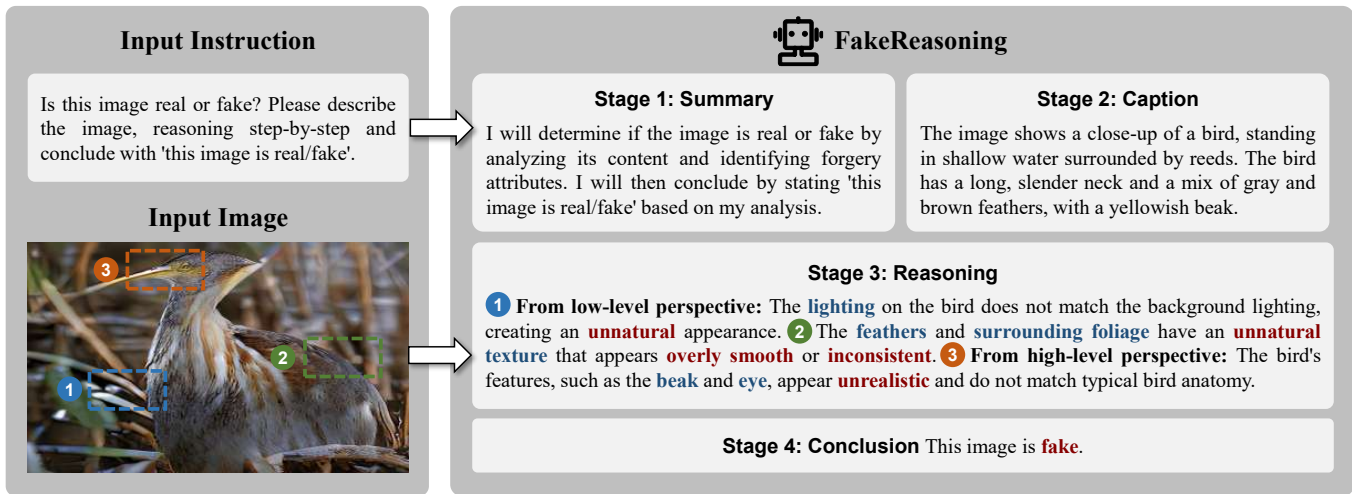


Fig. 1. Illustration of the FDR-Task. Different from traditional forgery detection, the FDR-Task leverages MLLMs to perform accurate detection through reliable reasoning over forgery attributes, improving both detection accuracy and interpretability.

language modeling by mapping the vocabulary probability distribution to classification scores, effectively bridging the optimization gap and improving detection performance. Our contributions can be summarized as follows:

- We formulate AI-generated image detection and explanation as a Forgery Detection and Reasoning task (FDR-Task), enabling models to jointly assess image authenticity and analyze forgery attributes.
- We introduce the Multi-Modal Forgery Reasoning Dataset (MMFR-Dataset), a large-scale dataset with comprehensive reasoning annotations, facilitating both training and evaluation of MLLM-based forgery detectors.
- We propose FakeReasoning, a forgery detection and reasoning framework that enhances fine-grained visual perception of MLLMs and couples language modeling task with forgery detection.
- Extensive experiments across generative models demonstrate that FakeReasoning not only achieves robust generalization but also outperforms state-of-the-art methods in both detection accuracy and interpretability.

II. RELATED WORK

In this section, we review recent advances in forgery detection and multi-modal large language models, analyze the motivation for integrating MLLMs into forgery detection, and summarize the limitations of existing approaches.

A. AI-Generated Image Detection

With the emergence of diverse generative models, it's crucial to design detectors generalizing to unseen domains. Traditional methods focus on uncovering low-level artifacts shared across generative models. CnNDetection [19] demonstrates that the detector trained on ProGAN [20] images exhibits strong generalization across GAN-generated images. GAN fingerprint [21] enables the attribution and detection of GAN-generated images by learning the unique fingerprints.

In the meanwhile, DIRE [22] indicates that diffusion-model-generated images can be well-reconstructed through pretrained diffusion models, whereas the reconstruction of real images is hard. Based on the finding, FakeInversion [23] uses original images, latent noise maps and reconstructed latent images for training. DRCT [24] creates hard examples by reconstructing real images and jointly conducts contrastive learning and binary classification on both original and reconstructed images. These methods achieve good intra-domain generalization but struggle to generalize across unseen domains.

Recently, high-level semantics has been explored using vision-language models to detect semantics inconsistencies within AI-generated images. UniDF [12] uses a frozen CLIP visual encoder [25] to avoid the mode asymmetry. DE-FAKE [26] observes that fake images tend to exhibit higher similarity to their captions than real images, and leverages CLIP's visual and text encoders to extract multi-modal features for training. FatFormer [13] follows zero-shot inference of CLIP, enhancing the prompt template with image embeddings and calculating cosine similarity for contrastive learning. Although vision-language models excel at capturing global semantic representations, it struggles to model low-level artifacts through image-text alignment pretraining.

B. Multi-Modal Large Language Models

Multi-modal large language models have emerged as a powerful tool for vision-language understanding. Instruction-following MLLMs like InstructBLIP [27], MiniGPT-4 [28] and LLaVA [29]–[31] introduce multi-modal adapters or projection layers on top of powerful LLMs (e.g., Vicuna [32], LLaMA [33]). These models enable sophisticated visual reasoning and dialogue, supporting tasks such as image captioning, visual question answering, and visual reasoning.

Recent advances in MLLMs reveal several trends across representative models such as Qwen-2.5-VL [34], GLM-4V [35], and InternVL [36]. First, there is a clear emphasis on scalable

TABLE I
COMPARISON WITH EXISTING DATASETS. GENERATORS DENOTES THE NUMBER OF GENERATIVE MODELS.

Dataset	Reference	Field	Annotator	Latest Generator	Generators	Images	Annotations
DD-VQA [15]	2024 ECCV	Deepfakes	Human	NeuralTextures [38] (2019)	4	3K	14K
FFA-VQA [16]	2024 arXiv	Deepfakes	GPT-4o	GANDiffFace [39] (2023)	7	95K	20K
Fakebench [40]	2024 arXiv	General	GPT-4V	DALLE3 [41] (2023)	10	3K	57K
LOKI [42]	2025 ICLR	General	Human	FLUX [43] (2024)	10	2K	0.2K
MMTD-Set [17]	2025 ICLR	General	GPT-4o	RePaint [44] (2022)	2	150K	34K
SID-Set [18]	2025 CVPR	General	GPT-4o	FLUX [43] (2024)	2	300K	3K
SynthScars [45]	2025 arXiv	General	Human	DALLE3 [41] (2023)	10	12K	26K
MMFR-Dataset	Ours	General	GPT-4o	GPT-4o (2025)	10	120K	378K

visual encoders capable of preserving high-resolution spatial information, either through dynamic resolution handling or high-capacity vision transformers. Second, these models increasingly adopt enhanced cross-modal fusion mechanisms, replacing lightweight adapters with more expressive modules, such as MLP-based mergers, gated activation functions, or large-scale query-driven cross-attention, to better align visual and textual features. Besides, DeepSeek-VL2 [37] integrates a Mixture-of-Experts (MoE) language model for efficient and scalable multi-modal reasoning. It employs sparsely activated expert routing, activating only a subset of parameters during inference.

With MLLMs’ strengths in cross-modal alignment and text generation, they have shown growing potential in forgery detection through detecting semantic inconsistencies and explaining suspicious visual cues.

C. Explainable Forgery Detection

To enhance the interpretability of forgery detection, localization has been introduced. Noiseprint [46] and TruFor [6] employ noise patterns to identify tampered regions. HiFi-Net [47] leverages the hierarchical relationships among generators as priors to enable fine-grained manipulation localization. However, localization-based methods often suffer from high false positive rates on authentic images. Moreover, with the rapid advancement of generative models, every pixel in an AI-generated image is synthesized, rendering saliency-based detectors ineffective.

As mentioned above, MLLMs acquire strong image understanding capabilities through large-scale image-text alignment pretraining. Empowered by large language models, MLLMs further gain text generation abilities, offering a new paradigm for forgery detection and interpretability. AntifakePrompt [48] redefines forgery detection as a visual question answering problem, using prompt tuning to fine-tune InstructBLIP [27]. Bi-LORA [49] formulates forgery detection as a image captioning task, using LoRA [50] to fine-tune BLIP-2 [51]. Built upon LISA [52], FakeShield introduces the $\langle \text{SEG} \rangle$ token as a mask embedding to guide the SAM decoder in localizing tampered regions. It interprets forgery detection results from both textual analysis and tampering localization perspectives. Similarly, SIDA [18] further introduces the $\langle \text{DET} \rangle$ token to supervise tampering localization and forgery detection tasks. However, most open-source MLLMs employ pretrained CLIP

as their visual encoder, resulting in poor sensitivity to low-level artifacts. Moreover, current MLLM-based detectors either optimize forgery detection with original language modeling task or add an external classification head, overlooking the inherent coupling between forgery detection and reasoning. These methods constrain the forensics potential of MLLMs in both detection accuracy and interpretability.

III. MULTI-MODAL FORGERY REASONING DATASET

To perform the proposed FDR-Task, high-quality images with forgery-related annotations are essential. Recently, several datasets have been developed to evaluate [40], [42] or fine-tune MLLMs [15]–[18], [45]. However, as summarized in Table I, existing datasets still face several challenges: 1) Insufficient annotations: current datasets either serve as benchmarks which lack enough samples for training or contain far fewer annotations compared to images, limiting the exploitation of MLLMs’ forensics capabilities. 2) Object-centric focus: datasets such as MMTD-Set [17] and parts of SID-Set [18] target tampered images with explicit manipulated masks, which neglecting holistic image analysis and limiting model generalizability.

To address these challenges, we propose the MMFR-Dataset, a large-scale synthetic image dataset with detailed annotations over forgery attributes. Leveraging GPT-4o and a customized data construction pipeline, we generate a substantial number of samples with comprehensive reasoning annotations. Each annotation is further organized in a structured (four-stage) and hierarchical (low-level and high-level) format, enabling a forgery reasoning chain-of-thought.

A. Source Image Collection

Training set: We follow the widely used “train-on-one and test-on-many” paradigm [53] in AI-generated image detection [12], [19]. For fake images, we choose DiffusionDB dataset [54]. Different from large-scale, automatically generated datasets, DiffusionDB collects well-crafted images generated by Stable Diffusion users on Discord, ensuring both generation quality and content diversity. For real images, we use LAION-Aesthetics v2 dataset [55].

Evaluation sets: In order to comprehensively evaluate the generalization of forgery detectors, we curate a collection of recent open-source AI-generated image datasets. Each

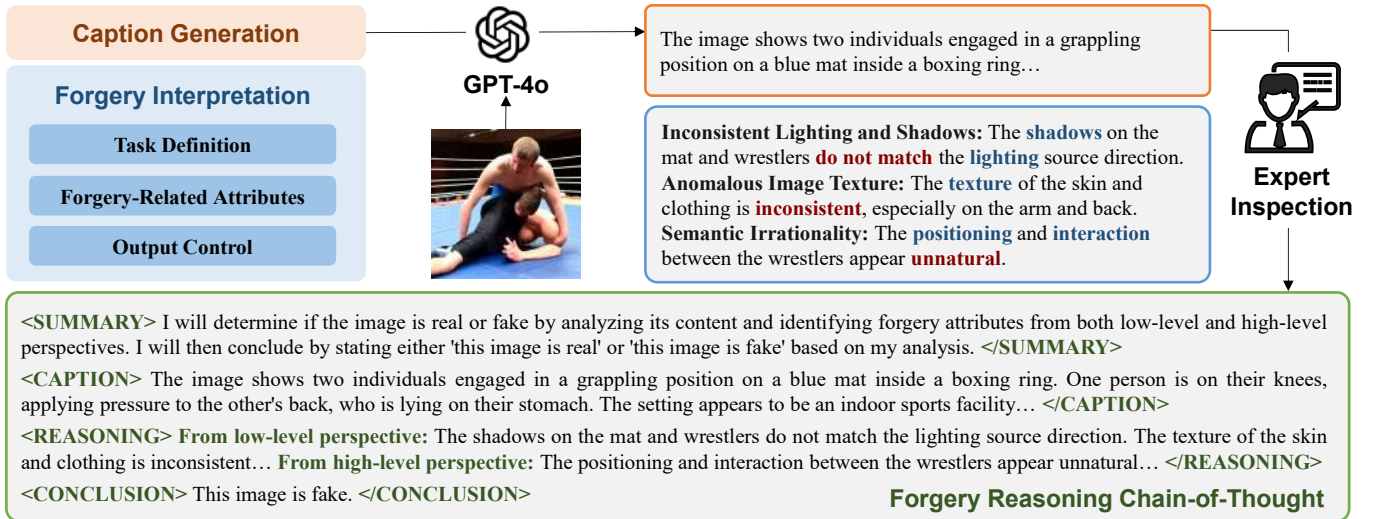


Fig. 2. Construction pipeline of the MMFR-Dataset. GPT-4o is tasked with caption generation and forgery interpretation. For the forgery interpretation task, the prompt is crafted to instruct GPT-4o to analysis forgery-related attributes. After inspected by human experts, the generated captions and interpretations are compiled with a chain-of-thought to enhance structured and hierarchical reasoning.

evaluation set comprises 1,000 fake images generated by state-of-the-art models released within the past three years, including: Stable Diffusion [54], DALLE-3 [56], DeepFloyd IF [48], Midjourney [57], Kandinsky [58], PixArt- α [59], FLUX [60], GPT-4o [61], StyleGAN-XL [48], and GigaGAN [62]. To ensure distributional consistency between real and fake images, we also collect 1,000 real images from ImageNet [63] and 1,000 from LAION [55]. ImageNet serves as the real set for StyleGAN-XL, while LAION is used for the others.

B. Forgery Reasoning Generation

Forgery reasoning annotations in the MMFR-Dataset is generated in two steps. First, we design a *Forgery Interpretation Prompt* and employ GPT-4o to interpret specific attributes signifying the image authenticity. Second, we decompose the process into four structured stages, with the reasoning stage further divided into two perspectives. The construction flow is shown in Figure 2.

1) *GPT-4o Assisted Forgery Interpretation:* GPT-4o has proven its capabilities in detecting and interpreting potential forgeries within images [40], [64]. Compared with manual analysis, employing GPT-4o for automated generation significantly expands the size of datasets, which is widely adopted in instruction tuning [29] and domain-specific fine-tuning [17], [65]. To generate precise and comprehensive analysis of forgery-related attributes, we design a *Forgery Interpretation Prompt* considering following aspects:

Task definition. First of all, the *Prompt* specifies the image authenticity as either “real” or “fake”. GPT-4o is tasked with identifying specific attributes that signify the image authenticity and providing detailed descriptions.

Forgery-related attributes. The *Prompt* includes a comprehensive set of attributes widely used in image forensics, ranging from low-level artifacts to high-level semantics, instructing

GPT-4o to focus on specific features indicative of image authenticity.

Output Control. The *Prompt* defines a json format including not only forgery attributes but also the authenticity label, which serves to enhance GPT-4o’s analysis on specific types. Besides, the *Prompt* also specifies a distinct output for failure cases where GPT-4o is unable to ascertain the image authenticity. Such outputs are filtered out after generation.

Upon generation, interpretations on forgery-related attributes are reviewed by human experts. And invalid annotations are filtered out.

2) *Forgery Reasoning Chain-of-Thought:* Inspired by recent advances in multi-modal chain-of-thought [66]–[68], we develop a specific chain-of-thought for forgery reasoning task, consisting of structured stages and hierarchical steps, to enhance forgery reasoning capability of MLLMs. First, we decompose the whole process into four stages:

Summary. In this stage, the *Forgery Reasoning CoT* provides a brief summary of the FDR-Task and explains the steps to conduct the whole process.

Caption. The *Forgery Reasoning CoT* gives a description of elements and relations within an image to help understand image and find forgeries.

Reasoning. The interpretations generated by GPT-4o are further organized into low-level and high-level reasoning perspectives based on the types of forgery attributes. Note that, since current MLLMs struggle with low-level perception, the hierarchical reasoning steps in the *Forgery Reasoning CoT* provide an effective supervision to the feature extraction of the dual-branch visual encoder in the proposed method.

Conclusion. Based on above stages, the *Forgery Reasoning CoT* outputs the final decision on image authenticity.

To emphasize structured reasoning stages, we use four pairs of special `<SEG>` tags: `<SUMMARY></SUMMARY>`, `<CAPTION></CAPTION>`, `<REASONING></REASONING>` and

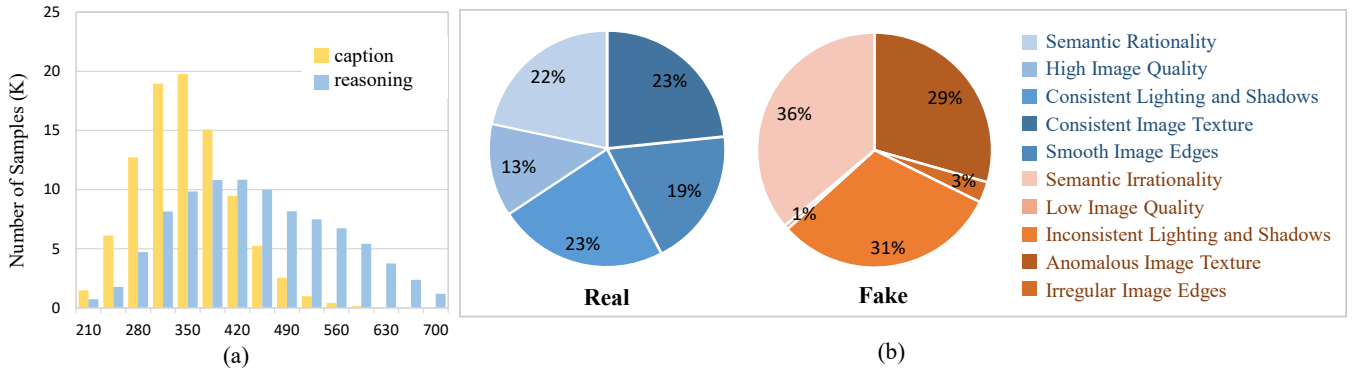


Fig. 3. Statistics of the MMFR-Dataset. (a) Text length distribution of caption and reasoning stages; (b) Attributes distribution of real and fake images.

<CONCLUSION></CONCLUSION> at both beginning and end of each stage. Summary and conclusion are predefined for the FDR-Task. Upon training on the MMFR-Dataset, MLLMs are able to conduct structured reasoning without external prompt engineering.

C. Dataset Statistics

The training set of the MMFR-Dataset consists of 50,266 synthetic images with 129,345 reasoning annotations, and 50,990 real images with 183,082 reasoning annotations. Across all annotations, there are 10 types of forgery-related attributes, whose distributions in real and fake images are depicted in Figure 3. Also, the figure shows the distribution of text length of both caption and reasoning stages.

The evaluation sets of the MMFR-Dataset comprise 10,000 synthetic images with 25,054 reasoning annotations and 10,000 real images with 41,726 reasoning annotations, providing the foundation for comprehensive evaluation of the FDR-Task.

IV. FAKEREASONING

The pipeline of FakeReasoning is illustrated in Figure 4. To enhance the fine-grained perception of MLLMs, FakeReasoning adopts a dual-branch visual encoder combining CLIP and DINO to extract both high-level and low-level visual clues. Each encoder is followed by an adapter to align with the text embedding. The Forgery-Aware Feature Fusion module (FAFF) further fuses CLIP tokens and DINO tokens with cross-attention mechanism, leveraging DINO’s attention maps as forgery-aware priors. This design adaptively guides MLLMs’ attention on low-level and high-level clues while highlighting potential forgery regions and entities. The Classification Probability Mapper (CPM) locates the classification token indicating the image authenticity from original logits and maps the vocabulary probability distribution into a classification score, which effectively couples language modeling with forgery detection and improves overall performance.

A. Dual-Branch Visual Encoder

To analyze the authenticity of an image, both low-level features (e.g., texture, edges, lighting) [69]–[71] and high-level semantics are essential [12]–[14]. Most existing open-source MLLMs [27]–[29] adopt pretrained CLIP as their visual

encoder. Although CLIP encoder excels at capturing global semantic representations, it lacks sensitivity to low-level visual clues due to image-text alignment pretraining [72]–[74], which poses a major limitation for MLLMs in image forensics.

Meanwhile, DINO [75] is pretrained through vision-only self-supervised learning, demonstrating strong capability in local perspective. Prior work has shown that integrating DINO features with CLIP features enhances fine-grained perception and mitigates hallucinations of MLLMs [76], [77]. Inspired by these advances, we further explore this “feature complementarity effect” in MLLM-based image forensics.

Specifically, the image X_v is input into a frozen CLIP and DINO visual encoder to obtain visual embeddings. Since the CLIP encoder is pretrained with text supervision while the DINO encoder is not, we introduce separate MLP modules, A_C for CLIP and A_D for DINO, as adapters to align with textual embedding space. These two adapters account for the heterogeneous nature of the two encoders and facilitate more effective modality alignment. Accordingly, the visual tokens from CLIP F_C and DINO F_D are obtained as follows:

$$F_C = A_C(\text{CLIP}(X_v)), \quad (1)$$

$$F_D = A_D(\text{DINO}(X_v)). \quad (2)$$

B. Forgery-Aware Feature Fusion

Fusion strategies of MLLMs’ visual embeddings can be broadly categorized into three types: feature weighting, feature concatenation, and layer interaction. Feature weighting aims to assign importance scores to different visual embeddings, yet it suffers from the distributional mismatch between CLIP and DINO representations, and can degrade the instruction-following ability of pretrained MLLMs [76]. Feature concatenation directly merges different visual embeddings into a single representation, lacking the adaptability to guide MLLMs’ attention on complementary low-level artifacts and high-level semantics. Layer interaction methods facilitate cross-layer communication between the two visual branches, but they typically introduce substantial computational complexity and rely on manually selected layers [72], [77].

To address these limitations and obtain discriminative forgery features, we introduce a Forgery-Aware Feature Fusion

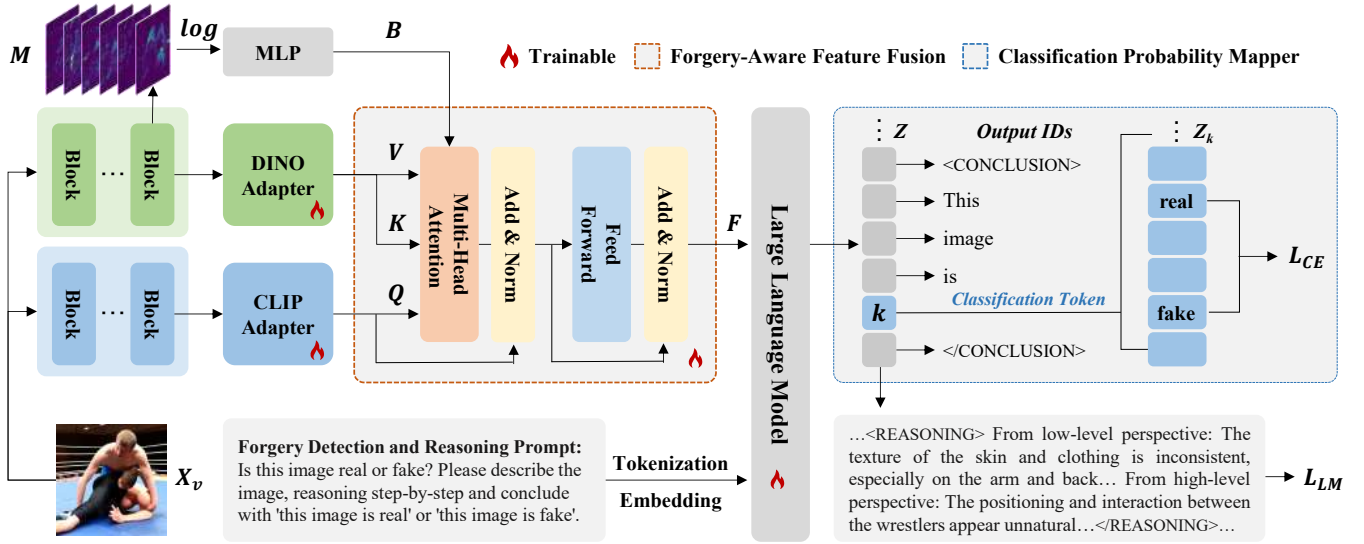


Fig. 4. The pipeline of FakeReasoning. FakeReasoning adopts a dual-branch visual encoder combining CLIP and DINO to extract both high-level and low-level visual clues. Each encoder is followed by an adapter to align with the text embedding. The Forgery-Aware Feature Fusion module further fuses CLIP tokens and DINO tokens with cross-attention mechanism, leveraging DINO’s attention maps as forgery-aware priors. The Classification Probability Mapper locates the classification token indicating the image authenticity from original logits and maps the vocabulary probability distribution into a classification score.

module, which leverages DINO’s attention maps as forgery-aware priors and applies a cross-attention mechanism to integrate CLIP and DINO visual representations. To start with, the final-layer attention maps $M \in \mathbb{R}^{n \times H \times L \times L}$ of the DINO visual encoder highlights H regions rich in semantic and entity-level information [78]. Leveraging this property, we use the attention maps M as forgery-aware priors and incorporate them into the cross-attention mechanism as the attention bias, highlighting potential forgery regions and entities. The attention bias B is computed as:

$$B = \text{MLP}(\log M), \quad (3)$$

where the logarithmic transformation aligns the scale of softmax-normalized attention maps and similarity logits [79]. The subsequent lightweight MLP contains two layers with a GELU non-linearity, which serves as a non-linear projection module that increases the representational capacity and enables head-specific modulation [80].

Using B as the attention bias, we take CLIP tokens $F_C \in \mathbb{R}^{n \times L \times d}$ as queries and DINO tokens $F_D \in \mathbb{R}^{n \times L \times d}$ as keys and values for cross-attention. Incorporating forgery-aware priors into fused feature F , the cross-attention is defined as:

$$A = \text{softmax}\left(\frac{F_C F_D^\top}{\sqrt{d}} + B\right), \quad (4)$$

$$F' = \text{LN}(A F_D + F_C), \quad (5)$$

$$F = \text{LN}(\text{FFN}(F') + F'), \quad (6)$$

where F_D^\top represents the transpose of the DINO tokens and FFN denotes the feed-forward network. Notably, the FAFF module employs H heads for cross-attention, consistent with the architecture of the CLIP and DINO visual encoders.

C. Classification Probability Mapper

In this section, we aim to explore the integration of MLLMs and forgery detection task. Existing MLLM-based detectors can be categorized into two types: 1) optimizing original language modeling task to indirectly improve detection accuracy [15], [17], [48], [49]; 2) training an independent classification head with intermediate features from MLLMs [16], [18], [81]. The first category overlooks the objective discrepancy between language modeling and forgery detection, resulting in suboptimal detection performance. And the second category, on the other hand, ignores the intrinsic connections between the textual interpretation and the classification result, thereby undermining the detector’s credibility.

To leverage the intrinsic connections between language modeling and forgery detection, we propose the Classification Probability Mapper. As illustrated in Figure 4, CPM locates the classification token indicating the image authenticity from original logits and maps the vocabulary probability distribution into a classification score. Specifically, the original logits $Z \in \mathbb{R}^{n \times N \times V}$ output from MLLMs represent the predicted probabilities of each token in the vocabulary, where N is the length of the output sequence and V is the size of the vocabulary. Using the Greedy Search Strategy [82], we sample the predicted words based on the highest probabilities and obtain the output IDs:

$$O = \arg \max_v(Z). \quad (7)$$

where the $\arg \max$ is taken over the vocabulary dimension $v \in \{0, 1, \dots, V - 1\}$ to obtain the output IDs $O \in \mathbb{R}^{n \times N}$.

According to the *Forgery Reasoning CoT*, image authenticity is determined in the conclusion stage. Therefore, we encode $\langle \text{CONCLUSION} \rangle$ and answer template “This image is” into token IDs as the match pattern p . We use this pattern

TABLE II

COMPARISON ON FORGERY DETECTION TASK. † DENOTES USING OFFICIAL WEIGHTS AND THE OTHERS ARE TRAINED ON THE MMFR-DATASET. SD, IF, MJ, KD, AND SG-XL REPRESENT STABLE DIFFUSION, DEEPFLOYD IF, MIDJOURNEY, KANDINSKY AND STYLEGAN-XL.

Method	Reference	SD	DALLE-3	IF	Mj	Kd	PixArt	FLUX	GPT-4o	SG-XL	GigaGAN	AVG
UniFD [12]	2023 CVPR	92.90	<u>88.80</u>	82.90	80.80	81.90	88.70	81.00	91.80	72.70	86.50	84.80
DE-FAKE [26]	2023 CCS	96.25	80.00	82.50	63.75	86.25	90.00	<u>86.25</u>	95.00	61.25	57.50	79.88
FatFormer† [13]	2024 CVPR	79.65	52.40	63.70	55.24	50.91	65.05	<u>37.56</u>	50.04	97.40	84.70	63.67
NPR [10]	2024 CVPR	98.80	50.90	72.60	94.60	91.90	86.50	49.90	74.40	79.80	77.90	77.73
DRCT† [24]	2024 ICML	75.30	70.40	71.90	75.76	65.31	75.56	81.71	74.81	82.65	58.65	73.21
FreqNet [83]	2024 AAAI	99.30	49.80	53.30	<u>93.90</u>	77.20	91.00	49.90	82.30	95.10	80.30	77.21
C2P† [14]	2025 AAAI	83.30	61.70	54.75	56.71	58.93	50.24	39.61	42.42	<u>96.70</u>	85.50	62.99
AIDE [84]	2025 ICLR	96.75	88.55	73.65	68.19	72.53	83.26	86.08	<u>95.51</u>	84.15	77.10	82.58
SPAI [9]	2025 CVPR	98.10	76.85	75.85	68.20	65.20	68.30	58.25	66.75	66.15	56.95	70.06
Effort† [85]	2025 ICML	93.50	66.15	<u>93.35</u>	80.76	<u>94.11</u>	<u>91.11</u>	79.97	76.50	96.55	<u>95.55</u>	<u>86.76</u>
FakeReasoning	Ours	<u>99.20</u>	91.28	99.10	87.68	96.90	93.49	87.16	97.80	90.00	98.00	94.06

to search through the output IDs and identify the index k of classification token:

$$k = \min\{i + l \mid O_{i:i+l} = p, i \in [0, N - l]\}, \quad (8)$$

where l is the length of the pattern p .

For the classification token, its logits corresponding to the vocabulary entries “real” and “fake” determine the image authenticity. Therefore, we model the forgery detection as a special case of multi-class classification, which is optimized with the cross-entropy loss:

$$\mathcal{L}_{CE} = -\log \frac{\exp(Z_{k, ID_y})}{\exp(Z_{k, ID_{\text{real}}}) + \exp(Z_{k, ID_{\text{fake}}})}, \quad (9)$$

where $y \in \{\text{real}, \text{fake}\}$ denotes the ground-truth label of image authenticity, $Z_{k, ID_{\text{real}}}$ and $Z_{k, ID_{\text{fake}}}$ denote the original logits of the classification token projected onto the vocabulary entries “real” and “fake”. To balance the scale of losses, we introduce a temperature hyperparameter τ to original logits in \mathcal{L}_{CE} by Z/τ , which is set to 10 in our experiment.

D. Joint Optimization

We use images and forgery reasoning annotations from the MMFR-Dataset as the visual input X_v and answers X_a . The question X_q , such as the Forgery Detection and Reasoning Prompt, is defined in Figure 4. Following the methodology of LLaVA [29], the language modeling task is optimized using an auto-regressive training objective:

$$\mathcal{L}_{LM} = -\sum_{j=1}^N \log p_{\theta}(x_j | X_v, X_{q, < j}, X_{a, < j}), \quad (10)$$

where θ represents the trainable parameters, $X_{q, < j}$ and $X_{a, < j}$ denote the question and answer tokens from all previous turns prior to the current prediction token x_j , and N is the sequence length. During training, FakeReasoning is optimized through joint losses:

$$\text{Loss} = \mathcal{L}_{CE} + \mathcal{L}_{LM}. \quad (11)$$

TABLE III

COMPARISON ON THE FDR-TASK. WE EMPLOY GPT-4O-ASSISTED FORGERY INTERPRETATIONS AS GROUND TRUTH AND ASSESS BOTH DETECTION AND REASONING TASKS.

Method	Detection				Reasoning		
	DM	GAN	AVG	Fail ↓	BL-1	R-L	CSS
LLaVA-1.5-13B [30]	<u>73.38</u>	70.85	<u>72.87</u>	0.00	0.23	0.20	0.54
Qwen-2.5-VL-7B [34]	63.58	54.37	61.74	3.70	0.22	0.19	0.56
InternVL-2.5-8B [36]	67.72	60.02	66.18	6.20	0.14	0.16	0.58
GLM-4V-9B [35]	68.91	67.31	68.59	3.35	0.11	0.14	0.61
Deepseek-VL2 [37]	68.46	67.59	68.29	<u>0.70</u>	<u>0.24</u>	<u>0.21</u>	<u>0.64</u>
FakeShield [17]	52.00	<u>80.00</u>	57.60	1.30	0.12	0.16	0.45
FakeReasoning	94.08	94.00	94.06	0.00	0.37	0.29	0.76

V. EXPERIMENT

In this section, we present a series of experiments to validate the effectiveness of the proposed method. We begin with implementation details, followed by the introduction of state-of-the-art baselines and evaluation metrics. Subsequently, we compare and analyze the results on two benchmark datasets. Finally, we provide visualization results and ablation studies to further demonstrate the strengths and limitations of our method.

A. Implementation Details

We adopt LLaVA-1.5-13B [30] as the base MLLM, and employ ViT-L/14 variants of CLIP [25] and DINO [75] as visual encoders. Our model is initialized with pretrained weights of LLaVA-MoF [76] for the LLM and the two adapters. During training stage, the visual encoders are frozen, while the LLM is fine-tuned using LoRA [50] with a rank of 128 and a scaling factor of 256. The adapters and the FAFF module are fully trainable. Our model is trained for 3 epochs on 8× NVIDIA A800 40GB GPUs with a batch size of 8. During inference, the temperature is set to 0.2.

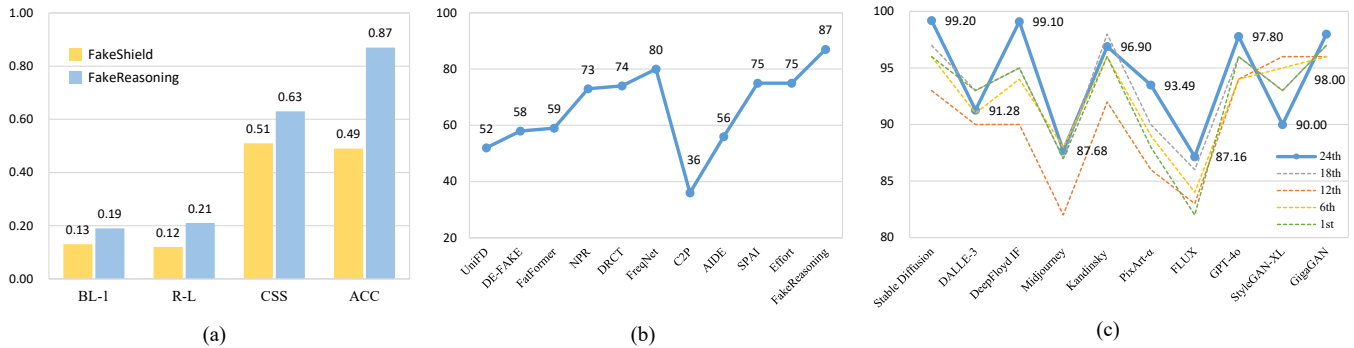


Fig. 5. (a) Evaluation of the FDR-Task on LOKI benchmark. (b) Detection evaluation on LOKI benchmark. (c) Ablation study on the layers.

B. Baseline models

We compare the detection performance of FakeReasoning and traditional detectors from three categories: 1) CLIP-based methods, including UniFD [12], DE-FAKE [26], FatFormer [13], C2P [14], and Effort [85]; 2) methods based on low-level features, such as NPR [10], DRCT [24], FreqNet [83], and SPAI [9]; and 3) hierarchical method AIDE [84] that integrates high-level and low-level features. For all baseline models, we either retrain them on the MMFR-Dataset or use their officially released weights.

Also, we compare detection and reasoning performance among FakeReasoning, open-source MLLMs and MLLM-based detectors. Specifically, open-source MLLMs include LLaVA-1.5-13B [30], Qwen-2.5-VL-7B [34], InternVL-2.5-8B [36], GLM-4V-9B [35], Deepseek-VL2 [37], while the MLLM-based detector FakeShield [17] is also included for comparison. All baseline models are reproduced and evaluated using their official weights.

C. Evaluation Metrics

For the forgery detection task, we report image-level accuracy (ACC), which is calculated based on the authenticity decisions in the conclusion stage. For the forgery reasoning task, we use GPT-4o-generated interpretations as the ground truth and evaluate performance using BLEU-1 [40], ROUGE-L [40], and Semantic Similarity (CSS) [17] metrics. The reasoning stage output of FakeReasoning is used for comparison.

D. Benchmark for FDR-Task

1) *Comparison on Forgery Detection Task:* We first conduct a comprehensive comparison on the generalization of detection task. As shown in Table II, the results include image-level accuracy for each evaluation set.

Compared to low-level-based methods such as NPR, DRCT, FreqNet, and SPAI, CLIP-based methods like UniFD, AIDE, DE-FAKE and Effort exhibit stronger cross-domain generalization. Despite being trained only on Stable Diffusion images, these models effectively detect GAN-generated contents. Low-level clues, e.g., frequency artifacts in FreqNet and SPAI or upsampling traces in NPR, vary across different generators, while the reconstruction error in DRCT is specific for diffusion models. In contrast, CLIP leverages strong semantic

priors to detect high-level inconsistencies, resulting in robust generalization. Trained on ProGAN images, FatFormer and C2P perform well on GAN-generated evaluation sets but suffer a substantial drop faced with diffusion models.

Besides, distinguishing fake images of FLUX and Midjourney proves to be more difficult. These commercial models have achieved a high degree of photorealism, posing increasing challenges to existing detection methods. We notice that when trained on Stable Diffusion images, several methods generalize surprisingly well on GPT-4o-generated images, including UniFD, DE-FAKE, AIDE and our method. We attribute this trend to similar distributions of two generators.

Meanwhile, our method outperforms all state-of-the-art baselines, with an average accuracy exceeding the suboptimal method Effort [85] by 7.3%. Specifically, our method achieves the highest accuracy in 7 out of 10 generative models and shows the smallest variation. With powerful prior knowledge and task-specific architecture, our method learns forgery semantics from both low-level and high-level visual clues, instead of generator-specific artifacts, which contributes to outstanding accuracy and strong generalization of our method.

2) *Comparison on FDR-Task:* To establish a foundational study for the FDR-Task, we employ GPT-4o-assisted forgery interpretations as the ground truth and assess the quality of forgery reasoning. We utilize the Forgery Detection and Reasoning Prompt, as illustrated in Figure 4, to query open-source MLLMs and MLLM-based detector. The results are presented in Table III. The “Fail” denotes cases where the MLLMs are unable to determine the authenticity of an image or fail to output in the required format.

Among open-source MLLMs, LLaVA-1.5-13B [30] demonstrates strong forgery detection capabilities and robust instruction-following behavior, while DeepSeek-VL2 [37] excels in forgery reasoning task. However, the overall performance of open-source MLLMs remains unsatisfactory. They suffer from domain shifts and uneven capabilities, limiting their applicability in real-world scenarios.

For the MLLM-based detector FakeShield [17], although it is trained on both GAN-generated and diffusion-edited images, it performs well on GAN-generated images but suffers a significant accuracy drop on diffusion-model-generated images, achieving only 52%. Further analysis reveals that FakeShield [17] attains 83.1% accuracy on fake images but only 33.6%

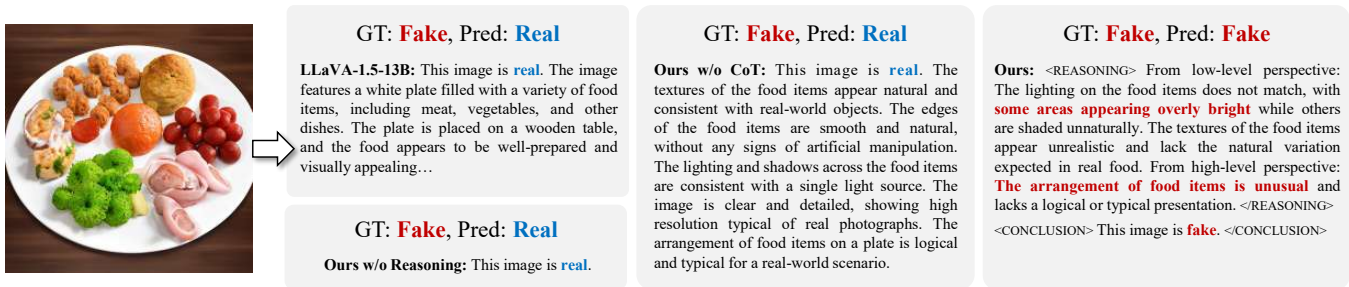


Fig. 6. Visual examples in the ablation study on forgery reasoning task. Only reasoning and conclusion stages of our method is presented. With the forgery reasoning chain-of-thought, our method achieves accurate detection through structured and hierarchical reasoning.

on real images, indicating a high false positive rate. Most existing image manipulation detection and localization models rely on semantic segmentation backbones that are not trained to differentiate between authentic and manipulated regions. Consequently, when applied to forgery detection tasks, they often misclassify authentic regions in real images as manipulation, resulting in a high false positive rate.

Our method achieves superior performance in both detection and reasoning tasks. Although trained solely on Stable Diffusion images, our method generalizes well to images generated by latest diffusion models and unseen GANs, exhibiting robust in-domain and cross-domain generalization capabilities. Moreover, by incorporating the *Forgery Reasoning CoT*, our method produces structured outputs containing clear authenticity judgments, which effectively reduces ambiguity and facilitates large-scale evaluation.

E. Evaluation on Existing Benchmarks

In this section, we choose LOKI [42] to evaluate both detection and reasoning ability of the baselines and our method. Specifically, we use all the images in LOKI to evaluate forgery detection task and use “open ended VQA” to evaluate forgery reasoning task. The results are shown in Figure 5.

On the LOKI benchmark, our method demonstrates superior reasoning capabilities compared to FakeShield [17]. We observe that our method exhibits a decline in BLEU-1 and ROUGE-L scores on the LOKI benchmark compared to the MMFR-Dataset. Through further analysis, we find that the 229 reasoning samples in the open-ended VQA comprises certain fake document images. These images differ significantly from natural images in reasoning patterns, resulting in reduced lexical coverage and disrupted word order alignment. Despite the inclusion of unseen domains such as documents, medical and satellite images, our method maintains robust detection performance on the LOKI benchmark, significantly outperforming FakeShield [17].

We further compare the detection performance of traditional detectors and our method. The LOKI benchmark includes fake images generated by ten state-of-the-art generative models, posing a great challenge for detectors. Among all methods, only FreqNet [83] and our method achieve over 80% detection accuracy, whereas the performance of other detectors remains suboptimal.

F. Ablation Study

1) *Ablation Study on Forgery Reasoning Task:* In this section, we try to validate that the FDR-Task, which couples visual reasoning with forgery detection, not only provides more explainable detection results, but also fully exploits MLLMs for image forensics. We design the following variants: 1) **Ours w/o Reasoning:** the variant takes “This image is real.” or “This image is fake.” as the ground truth output; 2) **Ours w/o CoT:** the variant takes original interpretations of GPT-4o as ground truth output. The performance of these variants is shown in Figure 6 and Table IV.

Fine-tuning MLLMs with simple binary answers could enhance their detection performance. However, this variant significantly constrains MLLMs’ reasoning capability, as it is difficult to align complex visual content with a binary label sentence. Conducting the reasoning task alongside detection not only enhances the quality of reasoning but also improves detection accuracy. Meanwhile, integrating *Forgery Reasoning CoT* further boosts both detection and reasoning performance. This structured process facilitates better alignment between visual and linguistic modalities, while hierarchical reasoning effectively leverages both high-level and low-level visual clues from the visual branch.

2) *Ablation Study on the Visual Branch:* In this work, we introduce a dual-branch visual encoder to enhance the fine-grained perceptual capability of MLLMs. To effectively integrate high-level and low-level visual clues, we propose a Forgery-Aware Feature Fusion module that enables discriminative feature learning for forgery detection. To validate the effectiveness of each component, we design several ablation variants. As shown in Table V, **CLIP** denotes using only the CLIP vision encoder; **CLIP+DINO** represents a simple interleaving of DINO and CLIP embeddings following [76]; **CLIP+DINO+CA** applies a cross-attention mechanism to fuse DINO and CLIP features; and **CLIP+DINO+CA+Bias** further incorporates DINO’s attention maps as the attention bias to guide the cross-attention integration. Since DINO is pretrained without textual supervision, using DINO alone struggles to align with LLMs, and thus a DINO-only variant is not included.

According to the results of **CLIP+DINO**, introducing the DINO encoder yields significant improvements in forgery detection. This confirms the feature-level complementarity

TABLE IV
ABLATION STUDY ON FORGERY REASONING TASK AND CPM.

Variants	Detection			Reasoning		
	DM	GAN	AVG	BL-1	R-L	CSS
LLaVA-1.5-13B [30]	73.38	70.85	72.87	0.23	0.20	0.54
Ours w/o Reasoning	90.25	93.50	90.90	0.0004	0.05	0.42
Ours w/o CoT	92.63	94.50	93.00	0.36	0.29	0.76
Ours w/o CPM	92.57	95.60	93.18	0.36	0.29	0.76
Ours	94.08	94.00	94.06	0.37	0.29	0.76

TABLE V
ABLATION STUDY ON THE VISUAL BRANCH. CA DENOTES CROSS ATTENTION MECHANISM. BIAS DENOTES ATTENTION BIAS.

CLIP	DINO	CA	Bias	Detection			Reasoning		
				DM	GAN	AVG	BL-1	R-L	CSS
✓	×	×	×	90.33	87.85	89.83	0.36	0.29	0.76
✓	✓	×	×	93.75	89.00	92.80	0.36	0.29	0.76
✓	✓	✓	×	90.38	96.00	91.50	0.36	0.29	0.76
✓	✓	✓	✓	94.08	94.00	94.06	0.37	0.29	0.76

between DINO and CLIP in MLLM-based forensics. Although **CLIP+DINO+CA** shows a slight accuracy drop, **CLIP+DINO+CA+Bias** achieves the best detection and reasoning performance by introducing DINO’s attention maps as forgery-aware priors. To further analysis the accuracy gain by the attention bias, we conduct an ablation study on the layer choice of DINO’s attention maps. Specifically, we extract attention maps from the 1st, 6th, 12th, 18th, and 24th layers of the pretrained DINO encoder and use them as the attention bias in FAFF module. The result are shown in Figure 5 (c).

Using the attention maps from the 24th layer achieves the highest average accuracy, outperforming other layers on 8 out of 10 generative models. In comparison, using the attention maps from the 12th layer results in a notable 3.46% decrease. These results indicate that leveraging high-level attention maps from DINO as the attention bias produces more discriminative fused features. We attribute this to two key factors. First, higher-layer attention maps tend to focus on semantically meaningful and context-aware regions, which can better highlight potential forgery areas and entities. Second, since CLIP and DINO features are first projected into semantic space via MLP layers, high-level attention aligns more effectively with the semantics of these adapted features.

3) *Ablation Study on CPM*: In our work, we propose the Classification Probability Mapper to better couple forgery detection with language modeling. As illustrated in Table IV, **Ours w/o CPM** denotes using only the language modeling objective without any classification guidance.

According to the results, the CPM module significantly improves the detection accuracy. Through probability mapping, the CPM module unifies the optimization objectives and enables coupling between forgery detection and language modeling. As a result, it not only mitigates the conflict between tasks but also achieves accuracy gain in forgery detection.

G. Visualization

We provide the forgery detection and reasoning results of the proposed FakeReasoning in Figure 7. Discriminate reasoning clues are bolded and corresponding regions in are highlighted within images.

As shown in the first two rows, FakeReasoning provides accurate detection results as well as reliable forgery reasoning from both high-level semantics and low-level artifacts. The third row shows representative failure cases. First, we analyze several fake images that are misclassified as real and find that these images often exhibit high visual fidelity. For example, in the first image of the third row, the shell texture is finely rendered, and both the hand structure and fingerprint details appear highly realistic, making it nearly impossible to distinguish even with the naked eyes. As generative models continue to advance, producing perfect fake images is easier than ever. Recent studies have demonstrated that MLLMs can perceive modalities beyond human vision, such as infrared and depth images [86], [87]. Inspired by these advances, our future work will investigate whether MLLMs can identify imperceptible artifacts and how to aligned artifacts with natural language.

Besides, we also analyze real images that are misclassified as fake, which can be broadly categorized into three types: 1) unconventional structures: as shown in the second image in the third row, the dog is positioned in a side-facing pose, revealing only one eye, with its dense fur obscuring the facial features, which deviates from the typical morphology of common dogs; 2) prominent foregrounds: typically captured with telephoto lenses that blur the background heavily, creating a visual pattern similar to generators’ lack of background realism, thus leading to misclassification; 3) abnormal texture: post-processing operations like sharpening or contrast enhancement cause texture deviations from typical distributions, interfering with the predictions. To address these issues, our future work will concentrate on expand data diversity, including complex distributions and post-processing operations.

H. More Analysis

1) *Consistency Analysis on Forgery Detection Task*: We perform consistency analysis on the detection results to assess potential inconsistencies in MLLM-based detectors. Specifically, we randomly sample 100 images from each evaluation set and run 100 inference rounds on these samples, with the initial temperature set to 0.2. The majority prediction is taken as the baseline, and the proportion of minority predictions is calculated to quantify inconsistency. The average inconsistency of forgery detection is 0.80%.

Temperature regulates randomness in text generation. Higher temperatures lead to more random and diverse outputs, while lower temperatures yield more deterministic and conservative results. We further evaluate the impact of temperature on inconsistency by setting it to 0.1, 0.2, 0.3 and 0.4. As the temperature increases, the inconsistency becomes more pronounced. The average inconsistency remains below 1% at temperatures of 0.1 and 0.2.

2) *Human Evaluation on Forgery Reasoning Task*: We conduct human evaluation on the reasoning outputs to assess



Fig. 7. Visualization results of FakeReasoning. Discriminate reasoning clues are bolded and corresponding regions are highlighted with dashed boxes.

potential hallucinations in MLLM-based detectors. Specifically, we randomly sample 100 images from each evaluation set, where both the ground-truth and predicted labels are fake. Each sentence in the forgery reasoning is scored using a 5-grade marking method by human experts, with 5 indicating highly rational and 1 indicating highly irrational. The average score is then computed for each evaluation set. The average rationality score for forgery reasoning is 4.19. And the results reveal a negative correlation between the rationality and the generative quality. When the generative quality is low, FakeReasoning provides detailed reasoning based on visual contents. As the generative quality increases, FakeReasoning tends to output more stereotypical reasoning results.

VI. CONCLUSION

In this paper, we introduced the FDR-Task, a framework that unifies detection and reasoning for AI-generated images. To support this, we proposed the MMFR-Dataset, a large-scale dataset with hierarchical forgery reasoning annotations. Leveraging this dataset, we developed FakeReasoning, which enhances both generalization and interpretability by adapting MLLMs’ visual branch and optimization to image forensics. Experiments on multiple generative models demonstrate that FakeReasoning consistently outperforms state-of-the-art methods in both detection and reasoning tasks.

VII. LIMITATION

As shown in the ablation study, the introduced modules in the visual branch have little impact on the metrics of

the reasoning task. Fully leveraging MLLMs for forgery reasoning, particularly the language branch, remains an open challenge. The inconsistencies and hallucinations inherent in LLMs can introduce risks that compromise the reliability of MLLM-based detectors. In future work, we aim to develop a forensics-oriented architecture for the language branch to further enhance the interpretability, consistency, and rationality of the forgery reasoning task. Furthermore, we plan to extend this approach to multi-modal forgery detection and improve robustness under real-world distribution shifts, thereby advancing more reliable verification systems for AI-generated content.

VIII. REFERENCES

REFERENCES

- [1] M. Momeni, “Artificial intelligence and political deepfakes: Shaping citizen perceptions through misinformation,” *Journal of Creative Communications*, vol. 20, no. 1, pp. 41–56, 2025.
- [2] P. Kaushik, V. Garg, A. Priya, and S. Kant, “Financial fraud and manipulation: The malicious use of deepfakes in business,” in *Deepfakes and Their Impact on Business*. IGI Global Scientific Publishing, 2025, pp. 173–196.
- [3] S. Mahony and Q. Chen, “Concerns about the role of artificial intelligence in journalism, and media manipulation,” *Journalism*, p. 14648849241263293, 2024.
- [4] Y. Liu, C. Xia, X. Zhu, and S. Xu, “Two-stage copy-move forgery detection with self deep matching and proposal superglue,” *IEEE Transactions on Image Processing*, vol. 31, pp. 541–555, 2021.
- [5] Y. Hua, R. Shi, P. Wang, and S. Ge, “Learning patch-channel correspondence for interpretable face forgery detection,” *IEEE Transactions on Image Processing*, vol. 32, pp. 1668–1680, 2023.

- [6] F. Guillaro, D. Cozzolino, A. Sud, N. Dufour, and L. Verdoliva, “Trufor: Leveraging all-round clues for trustworthy image forgery detection and localization,” in *Proceedings of the IEEE/CVF conference on computer vision and pattern recognition*, 2023, pp. 20 606–20 615.
- [7] Y. Li, Y. He, C. Chen, L. Dong, B. Li, J. Zhou, and X. Li, “Image copy-move forgery detection via deep patchmatch and pairwise ranking learning,” *IEEE Transactions on Image Processing*, 2024.
- [8] Y. Gao, W. Lin, J. Xu, W. Xu, and P. Chen, “Self-supervised adversarial training for robust face forgery detection,” in *BMVC*, 2023, p. 718.
- [9] D. Karageorgiou, S. Papadopoulos, I. Kompatsiaris, and E. Gavves, “Any-resolution ai-generated image detection by spectral learning,” in *Proceedings of the Computer Vision and Pattern Recognition Conference*, 2025, pp. 18 706–18 717.
- [10] C. Tan, Y. Zhao, S. Wei, G. Gu, P. Liu, and Y. Wei, “Rethinking the up-sampling operations in cnn-based generative network for generalizable deepfake detection,” in *Proceedings of the IEEE/CVF Conference on Computer Vision and Pattern Recognition*, 2024, pp. 28 130–28 139.
- [11] X. Fu, B. Fu, S. Chen, T. Yao, Y. Wang, S. Ding, X. Liang, and X. Li, “Faces blind your eyes: Unveiling the content-irrelevant synthetic artifacts for deepfake detection,” *IEEE Transactions on Image Processing*, 2025.
- [12] U. Ojha, Y. Li, and Y. J. Lee, “Towards universal fake image detectors that generalize across generative models,” in *Proceedings of the IEEE/CVF Conference on Computer Vision and Pattern Recognition*, 2023, pp. 24 480–24 489.
- [13] H. Liu, Z. Tan, C. Tan, Y. Wei, J. Wang, and Y. Zhao, “Forgery-aware adaptive transformer for generalizable synthetic image detection,” in *Proceedings of the IEEE/CVF Conference on Computer Vision and Pattern Recognition*, 2024, pp. 10 770–10 780.
- [14] C. Tan, R. Tao, H. Liu, G. Gu, B. Wu, Y. Zhao, and Y. Wei, “C2p-clip: Injecting category common prompt in clip to enhance generalization in deepfake detection,” in *Proceedings of the AAAI Conference on Artificial Intelligence*, vol. 39, no. 7, 2025, pp. 7184–7192.
- [15] Y. Zhang, B. Colman, X. Guo, A. Shahriyari, and G. Bharaj, “Common sense reasoning for deepfake detection,” in *European Conference on Computer Vision*. Springer, 2024, pp. 399–415.
- [16] Z. Huang, B. Xia, Z. Lin, Z. Mou, W. Yang, and J. Jia, “Ffaa: Multimodal large language model based explainable open-world face forgery analysis assistant,” *arXiv preprint arXiv:2408.10072*, 2024.
- [17] Z. Xu, X. Zhang, R. Li, Z. Tang, Q. Huang, and J. Zhang, “Fakeshield: Explainable image forgery detection and localization via multi-modal large language models,” *arXiv preprint arXiv:2410.02761*, 2024.
- [18] Z. Huang, J. Hu, X. Li, Y. He, X. Zhao, B. Peng, B. Wu, X. Huang, and G. Cheng, “Sida: Social media image deepfake detection, localization and explanation with large multimodal model,” in *Proceedings of the Computer Vision and Pattern Recognition Conference*, 2025, pp. 28 831–28 841.
- [19] S.-Y. Wang, O. Wang, R. Zhang, A. Owens, and A. A. Efros, “Cnn-generated images are surprisingly easy to spot... for now,” in *Proceedings of the IEEE/CVF conference on computer vision and pattern recognition*, 2020, pp. 8695–8704.
- [20] T. Karras, “Progressive growing of gans for improved quality, stability, and variation,” *arXiv preprint arXiv:1710.10196*, 2017.
- [21] N. Yu, L. S. Davis, and M. Fritz, “Attributing fake images to gans: Learning and analyzing gan fingerprints,” in *Proceedings of the IEEE/CVF international conference on computer vision*, 2019, pp. 7556–7566.
- [22] Z. Wang, J. Bao, W. Zhou, W. Wang, H. Hu, H. Chen, and H. Li, “Dire for diffusion-generated image detection,” in *Proceedings of the IEEE/CVF International Conference on Computer Vision*, 2023, pp. 22 445–22 455.
- [23] G. Cazenavette, A. Sud, T. Leung, and B. Usman, “Fakeinversion: Learning to detect images from unseen text-to-image models by inverting stable diffusion,” in *Proceedings of the IEEE/CVF Conference on Computer Vision and Pattern Recognition*, 2024, pp. 10 759–10 769.
- [24] B. Chen, J. Zeng, J. Yang, and R. Yang, “Drct: Diffusion reconstruction contrastive training towards universal detection of diffusion generated images,” in *Forty-first International Conference on Machine Learning*, 2024.
- [25] A. Radford, J. W. Kim, C. Hallacy, A. Ramesh, G. Goh, S. Agarwal, G. Sastry, A. Askell, P. Mishkin, J. Clark *et al.*, “Learning transferable visual models from natural language supervision,” in *International conference on machine learning*. PMLR, 2021, pp. 8748–8763.
- [26] Z. Sha, Z. Li, N. Yu, and Y. Zhang, “De-fake: Detection and attribution of fake images generated by text-to-image generation models,” in *Proceedings of the 2023 ACM SIGSAC Conference on Computer and Communications Security*, 2023, pp. 3418–3432.
- [27] W. Dai, J. Li, D. Li, A. M. H. Tiong, J. Zhao, W. Wang, B. Li, P. Fung, and S. Hoi, “Instructblip: Towards general-purpose vision-language models with instruction tuning,” *arXiv preprint arXiv:2305.06500*, 2023.
- [28] J. Chen, D. Zhu, X. Shen, X. Li, Z. Liu, P. Zhang, R. Krishnamoorthi, V. Chandra, Y. Xiong, and M. Elhoseiny, “Minigt-v2: large language model as a unified interface for vision-language multi-task learning,” *arXiv preprint arXiv:2310.09478*, 2023.
- [29] H. Liu, C. Li, Q. Wu, and Y. J. Lee, “Visual instruction tuning,” *Advances in neural information processing systems*, vol. 36, 2024.
- [30] H. Liu, C. Li, Y. Li, and Y. J. Lee, “Improved baselines with visual instruction tuning,” in *Proceedings of the IEEE/CVF Conference on Computer Vision and Pattern Recognition*, June 2024, pp. 26 296–26 306.
- [31] H. Liu, C. Li, Y. Li, B. Li, Y. Zhang, S. Shen, and Y. J. Lee, “Llava-next: Improved reasoning, ocr, and world knowledge,” January 2024. [Online]. Available: <https://llava-vl.github.io/blog/2024-01-30-llava-next/>
- [32] W.-L. Chiang, Z. Li, Z. Lin, Y. Sheng, Z. Wu, H. Zhang, L. Zheng, S. Zhuang, Y. Zhuang, J. E. Gonzalez *et al.*, “Vicuna: An open-source chatbot impressing gpt-4 with 90%* chatgpt quality,” See <https://vicuna.lmsys.org> (accessed 14 April 2023), vol. 2, no. 3, p. 6, 2023.
- [33] H. Touvron, T. Lavril, G. Izacard, X. Martinet, M.-A. Lachaux, T. Lacroix, B. Rozière, N. Goyal, E. Hambro, F. Azhar *et al.*, “Llama: Open and efficient foundation language models,” *arXiv preprint arXiv:2302.13971*, 2023.
- [34] S. Bai, K. Chen, X. Liu, J. Wang, W. Ge, S. Song, K. Dang, P. Wang, S. Wang, J. Tang, H. Zhong, Y. Zhu, M. Yang, Z. Li, J. Wan, P. Wang, W. Ding, Z. Fu, Y. Xu, J. Ye, X. Zhang, T. Xie, Z. Cheng, H. Zhang, Z. Yang, H. Xu, and J. Lin, “Qwen2.5-vl technical report,” *arXiv preprint arXiv:2502.13923*, 2025.
- [35] T. GLM, A. Zeng, B. Xu, B. Wang, C. Zhang, D. Yin, D. Rojas, G. Feng, H. Zhao, H. Lai, H. Yu, H. Wang, J. Sun, J. Zhang, J. Cheng, J. Gui, J. Tang, J. Zhang, J. Li, L. Zhao, L. Wu, L. Zhong, M. Liu, M. Huang, P. Zhang, Q. Zheng, R. Lu, S. Duan, S. Zhang, S. Cao, S. Yang, W. L. Tam, W. Zhao, X. Liu, X. Xia, X. Zhang, X. Gu, X. Lv, X. Liu, X. Liu, X. Yang, X. Song, X. Zhang, Y. An, Y. Xu, Y. Niu, Y. Yang, Y. Li, Y. Bai, Y. Dong, Z. Qi, Z. Wang, Z. Yang, Z. Du, Z. Hou, and Z. Wang, “Chatglm: A family of large language models from glm-130b to glm-4 all tools,” 2024.
- [36] Z. Chen, J. Wu, W. Wang, W. Su, G. Chen, S. Xing, M. Zhong, Q. Zhang, X. Zhu, L. Lu *et al.*, “Internvl: Scaling up vision foundation models and aligning for generic visual-linguistic tasks,” in *Proceedings of the IEEE/CVF Conference on Computer Vision and Pattern Recognition*, 2024, pp. 24 185–24 198.
- [37] Z. Wu, X. Chen, Z. Pan, X. Liu, W. Liu, D. Dai, H. Gao, Y. Ma, C. Wu, B. Wang *et al.*, “Deepseek-vl2: Mixture-of-experts vision-language models for advanced multimodal understanding,” *arXiv preprint arXiv:2412.10302*, 2024.
- [38] J. Thies, M. Zollhöfer, and M. Nießner, “Deferred neural rendering: Image synthesis using neural textures,” *Acm Transactions on Graphics (TOG)*, vol. 38, no. 4, pp. 1–12, 2019.
- [39] P. Melzi, C. Rathgeb, R. Tolosana, R. Vera-Rodriguez, D. Lawatsch, F. Domin, and M. Schaubert, “Gandifface: Controllable generation of synthetic datasets for face recognition with realistic variations,” in *Proceedings of the IEEE/CVF International Conference on Computer Vision*, 2023, pp. 3086–3095.
- [40] Y. Li, X. Liu, X. Wang, S. Wang, and W. Lin, “Fakebench: Uncover the achilles’ heels of fake images with large multimodal models,” *arXiv e-prints*, pp. arXiv-2404, 2024.
- [41] J. Betker, G. Goh, L. Jing, T. Brooks, J. Wang, L. Li, L. Ouyang, J. Zhuang, J. Lee, Y. Guo *et al.*, “Improving image generation with better captions,” *Computer Science*. <https://cdn.openai.com/papers/dall-e-3.pdf>, vol. 2, no. 3, p. 8, 2023.
- [42] J. Ye, B. Zhou, Z. Huang, J. Zhang, T. Bai, H. Kang, J. He, H. Lin, Z. Wang, T. Wu *et al.*, “Loki: A comprehensive synthetic data detection benchmark using large multimodal models,” *arXiv preprint arXiv:2410.09732*, 2024.
- [43] Black Forest Labs, “Flux,” <https://github.com/black-forest-labs/flux>, 2024.
- [44] A. Lugmayr, M. Danelljan, A. Romero, F. Yu, R. Timofte, and L. Van Gool, “Repaint: Inpainting using denoising diffusion probabilistic models,” in *Proceedings of the IEEE/CVF conference on computer vision and pattern recognition*, 2022, pp. 11 461–11 471.
- [45] H. Kang, S. Wen, Z. Wen, J. Ye, W. Li, P. Feng, B. Zhou, B. Wang, D. Lin, L. Zhang *et al.*, “Legion: Learning to ground and explain for synthetic image detection,” *arXiv preprint arXiv:2503.15264*, 2025.

- [46] D. Cozzolino and L. Verdoliva, "Noiseprint: A cnn-based camera model fingerprint," *IEEE Transactions on Information Forensics and Security*, vol. 15, pp. 144–159, 2019.
- [47] X. Guo, X. Liu, Z. Ren, S. Grosz, I. Masi, and X. Liu, "Hierarchical fine-grained image forgery detection and localization," in *Proceedings of the IEEE/CVF Conference on Computer Vision and Pattern Recognition*, 2023, pp. 3155–3165.
- [48] Y.-M. Chang, C. Yeh, W.-C. Chiu, and N. Yu, "Antifakeprompt: Prompt-tuned vision-language models are fake image detectors," *arXiv preprint arXiv:2310.17419*, 2023.
- [49] M. Keita, W. Hamidouche, H. Bougueffa Eutamene, A. Taleb-Ahmed, D. Camacho, and A. Hadid, "Bi-lora: A vision-language approach for synthetic image detection," *Expert Systems*, vol. 42, no. 2, p. e13829, 2025.
- [50] E. J. Hu, Y. Shen, P. Wallis, Z. Allen-Zhu, Y. Li, S. Wang, L. Wang, and W. Chen, "Lora: Low-rank adaptation of large language models," *arXiv preprint arXiv:2106.09685*, 2021.
- [51] J. Li, D. Li, S. Savarese, and S. Hoi, "Blip-2: Bootstrapping language-image pre-training with frozen image encoders and large language models," in *International conference on machine learning*. PMLR, 2023, pp. 19730–19742.
- [52] X. Lai, Z. Tian, Y. Chen, Y. Li, Y. Yuan, S. Liu, and J. Jia, "Lisa: Reasoning segmentation via large language model," in *Proceedings of the IEEE/CVF Conference on Computer Vision and Pattern Recognition*, 2024, pp. 9579–9589.
- [53] Y. Yang, Z. Qian, Y. Zhu, O. Russakovsky, and Y. Wu, "D3: Scaling up deepfake detection by learning from discrepancy," in *Proceedings of the Computer Vision and Pattern Recognition Conference*, 2025, pp. 23 850–23 859.
- [54] Z. J. Wang, E. Montoya, D. Munechika, H. Yang, B. Hoover, and D. H. Chau, "Diffusiondb: A large-scale prompt gallery dataset for text-to-image generative models," *arXiv preprint arXiv:2210.14896*, 2022.
- [55] C. Schuhmann, R. Beaumont, R. Vencu, C. Gordon, R. Wightman, M. Cherti, T. Coombes, A. Katta, C. Mullis, M. Wortsman *et al.*, "Laion-5b: An open large-scale dataset for training next generation image-text models," *Advances in Neural Information Processing Systems*, vol. 35, pp. 25 278–25 294, 2022.
- [56] DALLE-3, <https://huggingface.co/datasets/christoforu/dalle-3-images>, 2023.
- [57] M. Zhu, H. Chen, Q. Yan, X. Huang, G. Lin, W. Li, Z. Tu, H. Hu, J. Hu, and Y. Wang, "Genimage: A million-scale benchmark for detecting ai-generated image," *Advances in Neural Information Processing Systems*, vol. 36, pp. 77 771–77 782, 2023.
- [58] Kandinsky, <https://huggingface.co/datasets/diffusers-parti-prompts/kandinsky-2-2>, 2023.
- [59] PixArt- α , <https://huggingface.co/datasets/PixArt-alpha/PixArt-Eval30K>, 2024.
- [60] FLUX, https://huggingface.co/datasets/lehdung/flux_generated, 2025.
- [61] GPT-4o, <https://huggingface.co/datasets/FreedomIntelligence/ShareGPT-4o-Image>, 2025.
- [62] D. Cozzolino, G. Poggi, R. Corvi, M. Nießner, and L. Verdoliva, "Raising the Bar of AI-generated Image Detection with CLIP," in *Proceedings of the IEEE/CVF Conference on Computer Vision and Pattern Recognition Workshops*, 2024, pp. 4356–4366.
- [63] O. Russakovsky, J. Deng, H. Su, J. Krause, S. Satheesh, S. Ma, Z. Huang, A. Karpathy, A. Khosla, M. Bernstein, A. C. Berg, and L. Fei-Fei, "ImageNet Large Scale Visual Recognition Challenge," *International Journal of Computer Vision (IJCV)*, vol. 115, no. 3, pp. 211–252, 2015.
- [64] Z. Zhang, H. Wu, C. Li, Y. Zhou, W. Sun, X. Min, Z. Chen, X. Liu, W. Lin, and G. Zhai, "A-bench: Are llms masters at evaluating ai-generated images?" *arXiv preprint arXiv:2406.03070*, 2024.
- [65] H. Tran, Z. Yang, Z. Yao, and H. Yu, "Bioinstruct: instruction tuning of large language models for biomedical natural language processing," *Journal of the American Medical Informatics Association*, vol. 31, no. 9, pp. 1821–1832, 2024.
- [66] H. Shao, S. Qian, H. Xiao, G. Song, Z. Zong, L. Wang, Y. Liu, and H. Li, "Visual cot: Advancing multi-modal language models with a comprehensive dataset and benchmark for chain-of-thought reasoning," *Advances in Neural Information Processing Systems*, vol. 37, pp. 8612–8642, 2024.
- [67] G. Xu, P. Jin, L. Hao, Y. Song, L. Sun, and L. Yuan, "Llava-ol: Let vision language models reason step-by-step," *arXiv preprint arXiv:2411.10440*, 2024.
- [68] M. Diao, L. Yang, H. Yin, Z. Wang, Y. Wang, D. Tian, K. Liang, and Z. Ma, "Driverx: A vision-language reasoning model for cross-task autonomous driving," *arXiv preprint arXiv:2505.20665*, 2025.
- [69] N. Zhong, Y. Xu, S. Li, Z. Qian, and X. Zhang, "Patchcraft: Exploring texture patch for efficient ai-generated image detection," *arXiv preprint arXiv:2311.12397*, 2023.
- [70] C. Dong, X. Chen, R. Hu, J. Cao, and X. Li, "Mvss-net: Multi-view multi-scale supervised networks for image manipulation detection," *IEEE Transactions on Pattern Analysis and Machine Intelligence*, vol. 45, no. 3, pp. 3539–3553, 2022.
- [71] Z. Lai, J. Li, C. Wang, J. Wu, and D. Jiang, "Lideepdet: Deepfake detection via image decomposition and advanced lighting information analysis," *Electronics*, vol. 13, no. 22, p. 4466, 2024.
- [72] Z. Luo, F. K. Gustafsson, Z. Zhao, J. Sjölund, and T. B. Schön, "Controlling vision-language models for multi-task image restoration," *arXiv preprint arXiv:2310.01018*, 2023.
- [73] Y. Cai, F. Yin, D. Hammou, and R. Mantiuk, "Do computer vision foundation models learn the low-level characteristics of the human visual system?" in *Proceedings of the Computer Vision and Pattern Recognition Conference*, 2025, pp. 20 039–20 048.
- [74] Z. He, P.-Y. Chen, and T.-Y. Ho, "Rigid: A training-free and model-agnostic framework for robust ai-generated image detection," *arXiv preprint arXiv:2405.20112*, 2024.
- [75] M. Caron, H. Touvron, I. Misra, H. Jégou, J. Mairal, P. Bojanowski, and A. Joulin, "Emerging properties in self-supervised vision transformers," in *Proceedings of the IEEE/CVF international conference on computer vision*, 2021, pp. 9650–9660.
- [76] S. Tong, Z. Liu, Y. Zhai, Y. Ma, Y. LeCun, and S. Xie, "Eyes wide shut? exploring the visual shortcomings of multimodal llms," in *Proceedings of the IEEE/CVF Conference on Computer Vision and Pattern Recognition*, 2024, pp. 9568–9578.
- [77] D. Jiang, Y. Liu, S. Liu, J. Zhao, H. Zhang, Z. Gao, X. Zhang, J. Li, and H. Xiong, "From clip to dino: Visual encoders shout in multi-modal large language models," *arXiv preprint arXiv:2310.08825*, 2023.
- [78] M. Oquab, T. Darcet, T. Moutakanni, H. Vo, M. Szafraniec, V. Khalidov, P. Fernandez, D. Haziza, F. Massa, A. El-Nouby *et al.*, "Dinov2: Learning robust visual features without supervision," *arXiv preprint arXiv:2304.07193*, 2023.
- [79] A. Vaswani, N. Shazeer, N. Parmar, J. Uszkoreit, L. Jones, A. N. Gomez, E. Kaiser, and I. Polosukhin, "Attention is all you need," *Advances in neural information processing systems*, vol. 30, 2017.
- [80] A. Dosovitskiy, L. Beyer, A. Kolesnikov, D. Weissenborn, X. Zhai, T. Unterthiner, M. Dehghani, M. Minderer, G. Heigold, S. Gelly, J. Uszkoreit, and N. Houlsby, "An image is worth 16x16 words: Transformers for image recognition at scale," *ICLR*, 2021.
- [81] X. Guo, X. Song, Y. Zhang, X. Liu, and X. Liu, "Rethinking vision-language model in face forensics: Multi-modal interpretable forged face detector," in *Proceedings of the Computer Vision and Pattern Recognition Conference*, 2025, pp. 105–116.
- [82] I. Sutskever, O. Vinyals, and Q. V. Le, "Sequence to sequence learning with neural networks," *Advances in neural information processing systems*, vol. 27, 2014.
- [83] C. Tan, Y. Zhao, S. Wei, G. Gu, P. Liu, and Y. Wei, "Frequency-aware deepfake detection: Improving generalizability through frequency space domain learning," in *Proceedings of the AAAI Conference on Artificial Intelligence*, vol. 38, no. 5, 2024, pp. 5052–5060.
- [84] S. Yan, O. Li, J. Cai, Y. Hao, X. Jiang, Y. Hu, and W. Xie, "A sanity check for ai-generated image detection," *arXiv preprint arXiv:2406.19435*, 2024.
- [85] Z. Yan, J. Wang, P. Jin, K.-Y. Zhang, C. Liu, S. Chen, T. Yao, S. Ding, B. Wu, and L. Yuan, "Orthogonal subspace decomposition for generalizable ai-generated image detection," *arXiv preprint arXiv:2411.15633*, 2024.
- [86] S. Jiang, Z. Chen, J. Liang, Y. Zhao, M. Liu, and B. Qin, "Infrared-llava: Enhancing understanding of infrared images in multi-modal large language models," in *Findings of the Association for Computational Linguistics: EMNLP 2024*, 2024, pp. 8573–8591.
- [87] J. Han, K. Gong, Y. Zhang, J. Wang, K. Zhang, D. Lin, Y. Qiao, P. Gao, and X. Yue, "Onellm: One framework to align all modalities with language," in *Proceedings of the IEEE/CVF Conference on Computer Vision and Pattern Recognition*, 2024, pp. 26 584–26 595.